Chinese Chemical Letters 33 (2022) 1032–1036

Contents lists available at ScienceDirect

Chinese Chemical Letters

journal homepage: www.elsevier.com/locate/cclet

Tunable phase transition, band gap and SHG properties by halogen replacement of hybrid perovskites [(thiomorpholinium)PbX_3, X = Cl, Br, I]

Simin Liu[1], Lei He[1], Yuzhen Wang, Pingping Shi*, Qiong Ye*

Jiangsu Key Laboratory for Science and Applications of Molecular Ferroelectrics and School of Chemistry and Chemical Engineering, Southeast University, Nanjing 211189, China

ARTICLE INFO

Article history:
Received 2 July 2021
Accepted 15 July 2021
Available online 22 July 2021

Keywords:
Phase transition
Band gap
Nonlinear optical
Organic-inorganic hybrid perovskite
Halogen replacement

ABSTRACT

By the replacement of halogen anion, three new multifunctional organic-inorganic hybrid perovskites (thiomorpholinium)PbX_3 (X = Cl, Br, I) were successfully synthesized and underwent reversible structural transformation above room temperature, accompanied by the anomalous change of dielectric constant. With the adjustment of the halogen anion from Cl to I in the inorganic skeleton, the space group is transformed from centrosymmetric space group $P2_1/c$ ((thiomorpholinium)$PbCl_3$) to chiral one $P2_12_12_1$ ((thiomorpholinium)$PbBr_3$, (thiomorpholinium)PbI_3) at room temperature. The ordered-disordered transition of organic cations and the change of hydrogen bonds with the increase of temperature lead to above-room-temperature phase transitions. Ultraviolet absorption and second-harmonic generation (SHG) measurements confirmed that both the band gap and SHG activity of (thiomorpholinium)PbX_3 (X = Cl, Br, I) crystals were tunable. The band gaps reveal a broadening trend with 3.532 eV, 3.410 eV and 3.175 eV along the Cl → Br → I series. This work provides an effective molecular design for multifunctional organic-inorganic perovskites.

Organic–inorganic hybrid perovskites (OHPs), combining the advantages of organic materials and inorganic materials, exhibit interesting properties to make them promising candidates for applications in optoelectronic devices, battery and energy storage [1–3]. OHPs adopt the ABX_3 structural frameworks where generally "A" is organic cation [4,5]. Due to the unusual flexibility of organic cation and various BX_3 frameworks, the OHP materials are diversiform and relatively thermal stable. The design of functional compounds has become an important challenge in OHP material science [6].

OHPs based on group IV metals (Ge, Sn and Pb) are expected to exhibit semiconducting behavior and also play an important role in phase transition materials due to the presence of flexible organic components [7]. A tunable band gap, E_g, is one of the ideal semiconductor characteristics where the value of E_g can be tailored within the ideal range by the choice of halogen in the perovskite architecture [2]. For instance, the band gap of acentric hybrid perovskite $NH(CH_3)_3SnCl_3$ which shows three phase transitions is 3.59 eV [8]. After replacing Cl atoms with Br, the value of band gap of $NH(CH_3)_3SnBr_3$ decreased to 2.76 eV. In addition, a series of mixed halide halobismuthates, $[NH_2(CH_2CH_3)_2]_3Bi(Cl_{1-x}Br_x)_6$ (x from 0 to 1), show that the band gap change from 3.26 eV to 2.81 eV and nonlinear optical capacities are different with increased Br inclusion [9]. In view of the influence of replacement of halogen anions, we propose to take advantage of the strategy of halogen replacement to manipulate the phase transition, band gap and quadratic nonlinear optical properties of materials for realizing the multifunctional application.

Herein, we chose thiomorpholine cations $[(C_4H_{10}NS)^+]$ as "A" embedded between inorganic chains, because only a very low activation energy is needed to change the conformation of such small annular organic cation [10–12]. Three new thermoresponsive materials, (thiomorpholinium)PbX_3 (X = Cl, Br, I), were successfully synthesized and were found to undergo structural phase transition through differential scanning calorimetry (DSC) measurements. The replacement of halogen anions did not change the one-dimensional chain packing mode of the inorganic components in crystals. But the space group changed from centrosymmetric $P2_1/c$ of (thiomorpholinium)$PbCl_3$ to chiral $P2_12_12_1$ of (thiomorpholinium)$PbBr_3$ and (thiomorpholinium)PbI_3 at room temperature. And the phase transition temperature has been greatly changed. The band gap and second-harmonic generation

* Corresponding authors.
E-mail addresses: ppshi@seu.edu.cn (P. Shi), yeqiong@seu.edu.cn (Q. Ye).
[1] These authors contributed equally to this work.

https://doi.org/10.1016/j.cclet.2021.07.039
1001-8417/

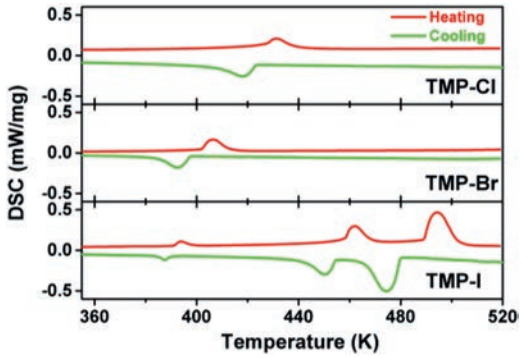

Fig. 1. The DSC curves for $(C_4H_{10}NS)PbX_3$ (X = Cl, Br, I).

(SHG) signal response of materials were also adjusted. The precise modification of the OHPs by halogen substitute of inorganic frame is proved to be an effective way to tune phase transition temperature, optical and electrical properties.

Crystals $(C_4H_{10}NS)PbCl_3$ (TMP-Cl), $(C_4H_{10}NS)PbBr_3$ (TMP-Br), $(C_4H_{10}NS)PbI_3$ (TMP-I) are prepared by slowly evaporating acid solution containing thiomorpholine and lead halides in a molar ratio of 1:1 for several days. The easy, low cost and low temperature processing through facile solution methods increases the possibility for the further practical applications of crystals. The phase purity was further verified by infrared spectroscopy (Fig. S1 in Supporting information) and powder X-ray diffraction (PXRD, Fig. S2 in Supporting information). The measured PXRD pattern matches well with the one simulated from the single-crystal X-ray diffraction structural data. Specific synthesis and test methods can be seen in Supporting information.

DSC measurements were carried out to determine the existence of reversible phase transitions below the melting point. For the three compounds, no thermal anomaly was found below 360 K. In the Fig. 1, a couple of exothermic (410.4 K) and endothermic (423.6 K) peaks indicate a reversible phase transition occurring in compound TMP-Cl. For TMP-Br, exothermic (398.4 K) and endothermic (401.4 K) peaks are clearly observed. The sharp peaks and the large heat hysteresis are the evidences of the first-order feature [13]. During the cooling and heating processes, three pairs of reversible heat anomalies at 390.5 K/392.7 K, 451.0 K/454.1 K, 488.7 K/480.4 K can be observed in the DSC curves of TMP-I, indicating three reversible phase transitions. On the basis of DSC results, the corresponding changes of total entropy (ΔS) of TMP-Cl and TMP-Br were calculated as ΔS_{Cl} (3.79 J mol^{-1} K^{-1}), ΔS_{Br} (4.46 J mol^{-1} K^{-1}). For TMP-I, the values of ΔS are 1.17, 7.07 and 16.24 J mol^{-1} K^{-1}, respectively. The halogen replacement of inorganic structure complicated the phase transition behavior. The change of phase transition temperature by halogen replacement provides a wider temperature range for the application of temperature-responsive materials.

Generally speaking, temperature-dependent dielectric response is also a preliminary test to examine the presence of phase transition [14–16]. As shown in Fig. 2, the temperature dependent real parts (ε') of compounds TMP-Cl, TMP-Br, TMP-I were measured in the heating–cooling cycles at 1 MHz. In the heating process, the ε' value of compound TMP-Cl increased gradually. Then the curve showed a turning point at around 414 K. In the cooling process, the dielectric anomaly appeared again at around 427 K, which confirmed the reversibility of phase transition in TMP-Cl. For compound TMP-Br, the ε' started at approximate 7.3 at 350 K in Fig. 2b. And the value of ε' showed a gradual increase with temperature increasing. Suddenly, it displayed a sharp increase to about 12.5. A step-like anomaly was seen at around 400 K. The ε' at the high dielectric state is about 1.2 times that at the low dielectric state. A

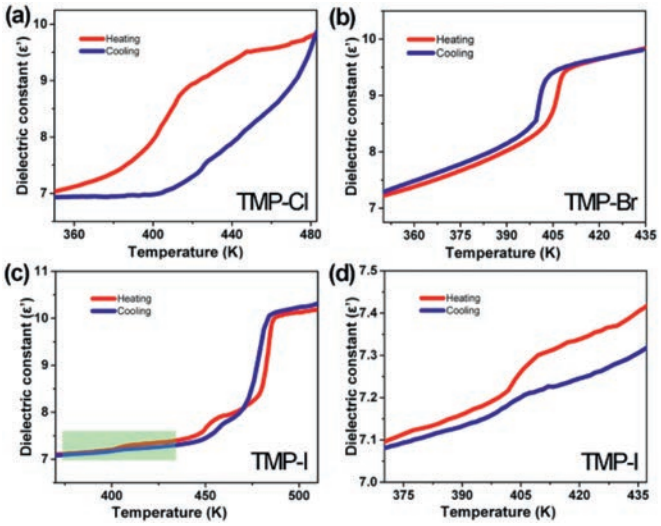

Fig. 2. Temperature-dependent real part (ε') of the dielectric constant measured at 1 MHz for (a) TMP-Cl, (b) TMP-Br, (c) TMP-I and (d) the partially enlarged curves of TMP-I at 1 MHz.

similar step-like anomaly can be seen in the cooling process, suggesting the occurrence of a reversible phase transition.

For compound TMP-I, three pairs of step-like anomalies were observed in Fig. 2c. During the heating process, dielectric anomalies appeared at about 401 K, 443 K and 478 K. There was a minor change of ε' at around 401 K, which was partially magnified in Fig. 2d. After further heating, the second dielectric anomaly appeared between 443 K and 460 K, and the value of dielectric constant changed obviously from 7.5 to 7.9. With further increase in temperature, the value of ε' increased sharply from 8.3 to 9.0 at around 478 K. During the process of cooling, the similar continuous step-like dielectric curve appeared again. The temperature-dependent dielectric responses for these three compounds were in good agreement with the DSC results mentioned above. Importantly, the dielectric responses of compounds TMP-Br and TMP-I can be regulated under two and four stable dielectric states, respectively. Due to such remarkable step-like dielectric anomalies, TMP-Br and TMP-I are expected to be promising switchable dielectric materials in a tunable temperature range [17,18]. In all, the halogen substitution of $(C_4H_{10}NS)PbX_3$ (X = Cl, Br, I) leads to multiple switching between different dielectric states.

The crystal structures of TMP-Cl, TMP-Br and TMP-I were analyzed in the room-temperature phase (RTP). The X-ray single crystal diffraction data was listed in the Table S1 (Supporting information). The room-temperature single crystal diffraction suggests that TMP- Cl belongs to the centrosymmetric monoclinic space group $P2_1/c$, with the cell parameters of a = 7.5615(7) Å, b = 7.7437(7) Å, c = 18.228(2) Å, $\alpha = \gamma = 90.000°$, β = 111.243(8)° and V = 994.80(18) $Å^3$. While both TMP-Br and TMP-I crystallize in the chiral orthorhombic space group $P2_12_12_1$, and the cell parameters are (TMP-Br: a = 7.9595(9) Å, b = 8.2785(10) Å, c = 16.4715(16) Å, $\alpha = \beta = \gamma = 90.000°$, V =1085.4(2) $Å^3$), (TMP-I: a = 8.3664 (7) Å, b = 8.7439(7) Å, c = 16.8371(13) Å, $\alpha = \beta = \gamma = 90.000°$, V = 1231.72(17) $Å^3$), respectively. As the halogen anions changed from Cl to I, the size of unit cell expanded at room temperature. With the change of space group from $P2_1/c$ to $P2_12_12_1$, the species of symmetry elements change from (E, C_2, i, σ_h) of TMP-Cl to (E, C_2, C'_2, C''_2) of TMP- Br and TMP-I. We can see that the inversion center (i) and glide plane (σ_h) disappear, and two-fold symmetry axes (C'_2, C''_2) emerge.

Structurally, the three compounds were found to be the typical ABX_3 organic-inorganic hybrid perovskite structure in the RTP.

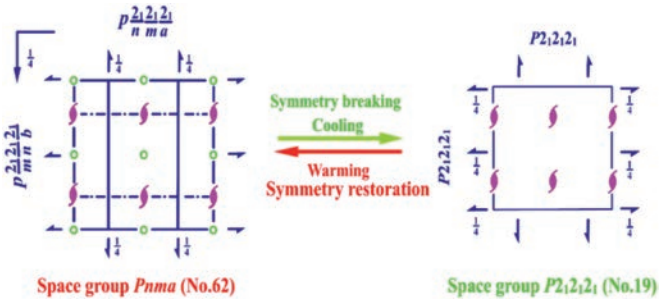

Fig. 3. Changes of spatial symmetry operations of compound TMP-Br between the HTP (*Pnma*) and RTP ($P2_12_12_1$).

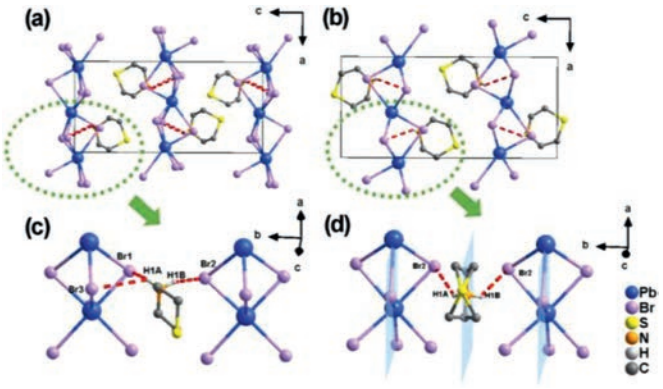

Fig. 4. For compound TMP-Br, packing structures viewed from the *b* axis in the (a) RTP and (b) HTP. The molecular structures in the (c) RTP and (d) HTP.

The asymmetric units of three compounds consist of one thiomorpholine cation, three halogen anions and one Pb cation. The halogen anions and Pb cations establish an octahedral geometry. PbX_6 (X = Cl, Br, I) octahedrons extend indefinitely and form a one-dimensional face-sharing chain lying on the two-fold axis. The lengths of Pb−X (X = Cl, Br, I) bonds control the size of inorganic framework. As listed in the Tables S2 and S3 (Supporting information), the Pb−Cl bond length ranges from 2.752(3) Å to 3.067(3) Å, which is shorter than Pb−Br (2.8656(17)-3.158(2) Å) and Pb−I (3.0604(7)-3.3348(8) Å). Longer Pb−X (X = Cl, Br, I) bonds provide more free space for the movement of organic cations, and also make TMP-Br and TMP-I exhibit a higher symmetry than TMP-Cl.

Given the DSC results that reveal the occurrence of phase transitions, crystal structures in the high-temperature phase (HTP) need to be further studied. When the temperature was increased to 423 K, the compound TMP-Br was transformed into the centrosymmetric orthorhombic space group *Pnma* with the cell parameters: a = 8.0028(17) Å, b = 8.1755(15) Å, c = 17.121(4) Å, $\alpha = \beta = \gamma$ = 90.000°, and V = 1120.2(4) Å^3. As shown in Fig. 3, from the RTP to HTP, the number of symmetry elements increased from four (E, C_2, C'_2, C''_2) to eight (E, C_2, $2C'_2$, i, σ_h, $2\sigma_v$). In the HTP, the asymmetric unit of TMP-Br comprises a half formula unit of $(C_4H_{10}NS)PbBr_3$.

From the RTP to HTP, the new mirror planes through the thiomorpholine cations and $(PbBr_3)_n^{n-}$ chains appeared as depicted in Fig. 4, instead of the two-fold symmetry axis at the center of $(PbBr_3)_n^{n-}$ chains in the RTP. The bond length of Pb−Br became 2.8684(11)–3.1218(8) Å, and the bond angle became 86.76(2)°–166.975(18)°. The inorganic chains changed slightly. For organic components, the thiomorpholine six-membered ring cations show chair-type conformation in the RTP. However, in the HTP, N and S atoms are located on the mirror planes. Some of the C atoms are distributed on both sides of the mirror planes, showing strong disorder motion in a twisted state. Meanwhile, the number of N−H···Br hydrogen bonds between organic and inorganic components reduced from three (N1−H1A···Br1, N1−H1A···Br3, N1−H1B···Br2) to two (N1−H1A···Br2, N1−H1B···Br2) with temperature increasing. Therefore, we can speculate that the phase transition of TMP-Br above room temperature is closely related to its hydrogen bonds and the ordered-disordered transition of thiomorpholine cations. Furthermore, the abundant hydrogen bonds of TMP-I may make an important contribution to its higher temperature phase transition.

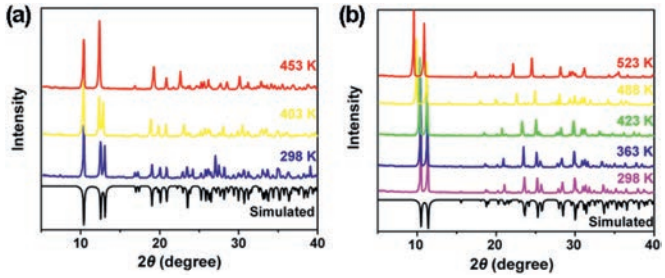

Fig. 5. Variable-temperature PXRD patterns of (a) TMP-Cl and (b) TMP-I.

We tried to collect the single-crystal structure of TMP-Cl and TMP-I in the high-temperature phase, but the crystal diffraction data was very poor. As a result, the variable temperature PXRD was measured to further verify the structural transformation at different temperatures. As shown in Fig. 5, the sample of TMP-Cl was measured at 298 K, 403 K and 453 K, respectively. At 403 K, the diffraction peaks of TMP-Cl are consistent with that at room temperature. The diffraction peaks at 12.33°, 12.99°, 16.83°, 17.28°, 19.96° existed at 403 K, but vanished at 453 K. In the meantime, new diffraction peaks emerged at 12.32°, 16.93°, 27.81°, 28.53°. Obviously, the number of diffraction peaks decreases at 453 K, indicating that the high-temperature structure has a higher symmetry. Among the results of Pawley refinements, the most possible space group of TMP-Cl at 453 K is *Cmcm* (Fig. S3 in Supporting information). For TMP-I, the PXRD was measured at 298, 363, 423, 488 and 523 K, respectively. At 423 K, the PXRD pattern of the TMP-I showed some changes. The diffraction peak at 31.65° disappeared and new peaks at 27.94°, 33.38° appeared. After the second phase transformation, the diffraction peaks at 15.54° and 25.364° disappeared. New diffraction peaks appeared at 14.07° and 32.14°. As the temperature increases to 523 K, the number of diffraction peaks decreases, indicating a highly symmetric lattice and severe molecular disorder at high temperature. Significant changes in PXRD patterns confirmed the presence of phase transitions in TMP-I. Combining the simulation results from Pawley refinements (Fig. S4 in Supporting information) with the crystal cell parameters obtained by single crystal diffractometer scanning at high temperature (Table S5 in Supporting information), the *Pnma, Pnma, Cmcm* space groups were suggested as the most possible ones at 423 K, 488 K, 523 K, respectively.

In order to further confirm and analyze the effects of halogen substitution on intermolecular interactions and structural phase transitions, Hirshfeld d_{norm} surfaces and 2D fingerprint plots were studied [19]. Hirshfeld d_{norm} surface was highlighted in red, indicating atoms make intermolecular contacts closer than the sum of their van der Waals radii. And white color denotes contacts around the sum of van der Waals radii. Longer contacts are blue [20–22].

In the Fig. 6, the difference of red dot regions on the Hirsfield d_{norm} surface map among TMP-Cl, TMP-Br and TMP-I indicates that the interactions between thiomorpholine cations and the surrounding molecules have been changed. As shown in the Figs. 6a–c, TMP-I has more abundant hydrogen bonds than those in TMP-Br and TMP-Cl at room temperature, which mainly involve C–H···X

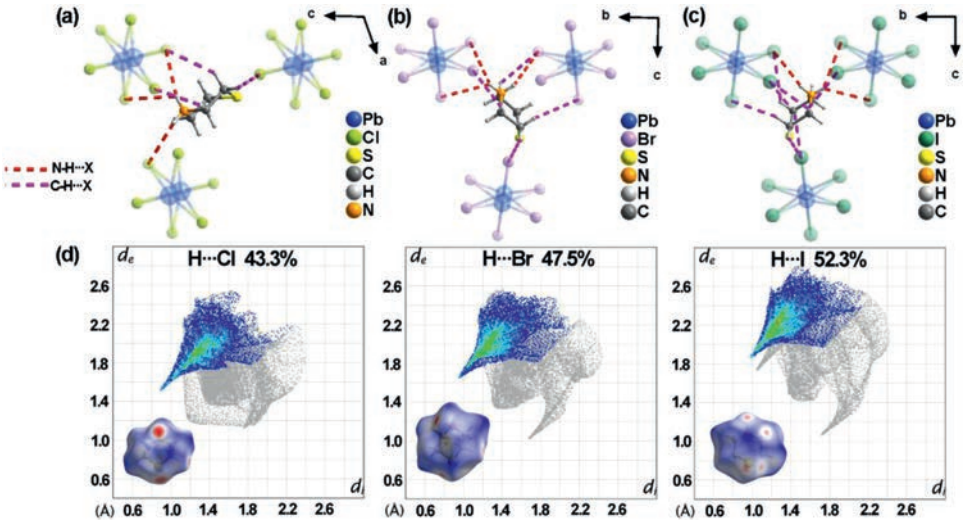

Fig. 6. Local H-bonded configurations of single thiomorpholine cation of (a) TMP-Cl, (b) TMP-Br and (c) TMP-I. (d) The Hirshfeld d_{norm} surfaces and the 2D fingerprint plots of the thiomorpholine cations in TMP-Cl, TMP-Br and TMP-I. (For interpretation of the references to color in this figure, the reader is referred to the web version of this article.).

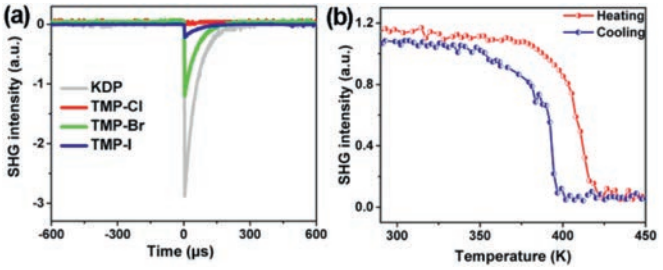

Fig. 7. (a) Oscilloscope traces of SHG signals for TMP-Cl, TMP-Br, TMP-I and KDP at the room temperature. (b) The SHG curves of TMP-Br at variable temperature.

and N–H···X (X = Cl, Br, I) bonds. Therefore, the Hirshfeld d_{norm} surfaces of the thiomorpholine cations in TMP-I have the most numerous red and white regions. The specific hydrogen bond parameters are listed in Table S4 (Supporting information). It can be inferred from Fig. 6d that H···X (X = Cl, Br, I) is the dominant interaction and responsible for the appearance of red part, whose percentage increased from 43.3% of TMP-Cl to 47.5% of TMP-Br. Then the proportion of TMP-I (52.3%) is the largest. It is worth noting that the halogen anions play an important part in the interactions. As temperature increases, it is the percentage of H···Br interactions for TMP-Br that underwent an evident change from 47.5% to 45.7% in the HTP (Fig. S5 in Supporting information), indicating the variation of the interactions between the thiomorpholine cations and surrounding $(PbBr_3)_n^{n-}$ chains alters the phase transition.

Because of the chiral structures and the high temperature phase transitions, this series of OHPs is expected to be SHG materials. Powder SHG measurements were performed based on Kurtz-Perry method with KH_2PO_4 (KDP) microcrystals serving as references in Fig. 7a. At room temperature, the SHG intensities of TMP-Br and TMP-I were estimated to be 0.37 and 0.09 times as large as that of KDP, respectively. The TMP-Cl crystal with the centrosymmetric space group in the RTP has no SHG signal (only the noise error was detected). The TMP-Br and TMP-I exhibit high SHG responses ("SHG-ON state") at room temperature [23–25]. As the temperature changes, the space group and crystal symmetry may also change to be reflected in the SHG response [26]. According to the results of the XRD diffraction measurement at 423 K, the space group of TMP-Br was transformed from the chiral $P2_12_12_1$ to the centrosymmetric *Pnma*. For TMP-Br, a step-like decrease of SHG intensity appeared in the vicinity of 423 K, and then it keeps about zero ("SHG-OFF") above the phase transition temperature (Fig. 7b). For TMP-I, no SHG signal was observed above 413 K (Fig. S6in Supporting information), which verifies the reliability of the proposed centrosymmetric space groups at high temperatures. During the heating and cooling cycle, the NLO switching between the "SHG-ON" and "SHG-OFF" states suggests that TMP-Br and TMP-I crystals are promising SHG switching materials. The halogen replacement of hybrid perovskites is one of the doable methods to find SHG switching materials.

The lead contained in the structure makes important contributions to potential semiconducting properties [7]. To further explore the semiconducting properties of compounds, the UV-vis absorption spectra of $(C_4H_{10}NS)PbX_3$ (X = Cl, Br and I) perovskites in the range from 200 nm to 700 nm (Fig. S7 in Supporting information) at room temperature were studied. The absorption edge of $(C_4H_{10}NS)PbX_3$ (X = Cl, Br and I) have a red-shifting tendency from 293 nm (TMP-Cl) to 326 nm (TMP-Br), to 364 nm (TMP-I).

The absorption region of organic-inorganic hybrid perovskite can be expanded by replacing halogen anions. It is well known that the absorption characteristics of materials are related to the type of band gap (direct band gap or indirect band gap). According to the Tauc equation $(hvF(R_\infty))^{1/n} = A(hv - E_g)$, where the value of n depends on the transition type of sample, $n = 2$ (indirect band gap) or 1/2 (direct band gap). Based on DFT, the band gaps of these systems are calculated to be 3.532 eV (TMP-Cl), 3.410 eV (TMP-Br) and 3.175 eV (TMP-I). The conduction-band minimum (CBM) and the valence-band maximum (VBM) lie at different positions in the Brillouin zone (Fig. 8, Figs. S8 and S9 in Supporting information). The calculation result indicates that they are all indirect band gap semiconducting materials. The values of the E_g estimated from the Tauc plot are 3.587 eV (TMP-Cl), 3.391 eV (TMP-Br) and 3.053 eV (TMP-I), which are close to the values calculated by DFT. The band gaps decrease along the Cl → Br → I series. The method of halogen replacement adjusts the band gap of (thiomorpholinium)PbX_3 (X = Cl, Br, I), which makes great contributions in the field of controllable semiconducting materials. Furthermore, the partial density of states (PDOS) of this series has also been calculated to better understand band gap allocation. As shown in Fig. 8b, Br 4s/p and Pb 6s/p played a major role in the band gap of TMP-Br. In other words, the inorganic chain-like construction $(PbX_3)_n^{n-}$

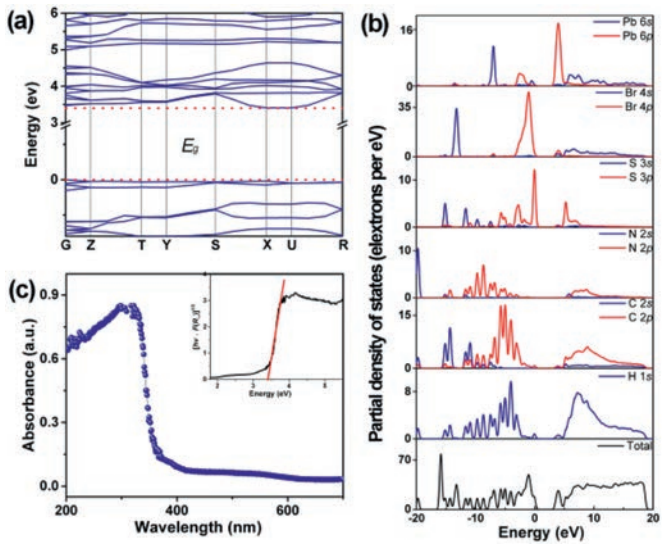

Fig. 8. (a) Calculated band structure and (b) PDOS of compound TMP-Br. (c) The UV–v is absorption spectrum and the Tauc plot show the band gap of compound TMP-Br.

(X = Cl, Br, I) is a significant factor for the semiconducting properties of this series.

To sum up, three organic–inorganic hybrid perovskites $(C_4H_{10}NS)PbX_3$ (X = Cl, Br, I) have been successfully synthesized and studied. The results of DSC and temperature-dependent dielectric constant reveal that the phase transition temperature could be tuned by the substitution of halogen anions. More than that, the centrosymmetric space group $P2_1/c$ (TMP-Cl) is also adjusted into the chiral space group $P2_12_12_1$ (TMP-Br, TMP-I) with detectable SHG response at room temperature. And the band gaps have varied from 3.532 eV to 3.410 eV, then to 3.175 eV with the increase of halogen anion radius. From the application standpoint, the band gap progression in the series $(C_4H_{10}NS)PbX_3$ (X = Cl, Br, I) will hold promise for highly tunable semiconductor for electronic and energy applications. Structurally, it has been revealed that the substitution of halogen anions promotes the formation of intramolecular hydrogen bonds, which further affects the physical properties. The substitution of halogen anions to achieve tunable physical properties provides useful guidance for the design of multifunctional optoelectronic materials.

Declaration of competing interest

The authors declare that they have no known competing financial interests or personal relationships that could have appeared to influence the work reported in this paper.

Acknowledgments

This work was financially supported by the National Natural Science Foundation of China (Nos. 21805033 and 21771037).

Supplementary materials

Supplementary material associated with this article can be found, in the online version, at doi:10.1016/j.cclet.2021.07.039. The supplementary crystallographic data for this paper have been uploaded in the Cambridge Structural Database. The number of CCDC are as follows: 2072739 (TMP-Cl at 298 K), 2072740 (TMP-Br at 298 K), 2072742 (TMP-Br at 423 K) and 2072743 (TMP-I at 298 K).

References

[1] W. Li, Z. Wang, F. Deschler, et al., Nat. Rev. Mater. 2 (2017) 16099.
[2] B. Saparov, D.B. Mitzi, Chem. Rev. 116 (2016) 4558–4596.
[3] N.J. Jeon, J.H. Noh, W.S. Yang, et al., Nature 517 (2015) 476–480.
[4] L. He, Y. Liu, P. Shi, et al., ACS Appl. Mater. Interfaces 12 (2020) 53799–53806.
[5] L. Zhou, P.P. Shi, X.M. Liu, et al., NPG Asia Mater. 11 (2019) 1–15.
[6] O. Sato, Nat. Chem. 8 (2016) 644–656.
[7] Y.J. Cao, L. Zhou, L. He, et al., Chem. Eur. J. 26 (2020) 14124–14129.
[8] Y. Dang, C. Zhong, G. Zhang, et al., Chem. Mater. 28 (2016) 6968–6974.
[9] X. Zheng, Y. Liu, G. Liu, et al., Chem. Mater. 28 (2016) 4421–4431.
[10] W.J. Xu, C.T. He, C.M. Ji, et al., Adv. Mater. 28 (2016) 5886–5890.
[11] J. Zhang, X. Liu, X. Li, et al., Chem. Asian J. 13 (2018) 982–988.
[12] A. Zeb, Z. Sun, A. Khan, et al., Inorg. Chem. Front. 5 (2018) 897–902.
[13] W.Q. Liao, Y.Y. Tang, P.F. Li, et al., J. Am. Chem. Soc. 139 (2017) 18071–18077.
[14] Y. Yu, P. Huang, Y. Wang, et al., Chin. Chem. Lett. 32 (2021) 3558–3561.
[15] Y. Xue, Z. Zhang, P. Shi, et al., Chin. Chem. Lett. 32 (2021) 539–542.
[16] L.H. Kong, D.W. Fu, Q. Ye, et al., Chin. Chem. Lett. 25 (2014) 844–848.
[17] L. He, L. Zhou, P.P. Shi, et al., Chem. Mater. 31 (2019) 10236–10242.
[18] S.M. Liu, Y.J. Cao, L. He, et al., Inorg. Chem. 59 (2020) 18396–18401.
[19] B. Hamdi, R. Zouari, A. Ben Salah, Chem. Pap. 72 (2018) 2795–2811.
[20] J.J. McKinnon, D. Jayatilaka, M.A. Spackman, Chem. Commun. (2007) 3814–3816.
[21] Y.T. Liu, L. He, P.P. Shi, et al., Chem. Commun. 56 (2020) 13764–13767.
[22] S.K. Wolff, D.J. Grimwood, J.J. Mckinnon, et al., CrystalExplorer (2007).
[23] X. Liu, C. Ji, Z. Wu, et al., Chem. Eur. J. 25 (2019) 2610–2615.
[24] H.Y. Shen, L. He, P.P. Shi, et al., J. Mater. Chem. C 9 (2021) 4338–4343.
[25] Z.B. Liu, L. He, P.P. Shi, et al., J. Phys. Chem. Lett. 11 (2020) 7960–7965.
[26] L. He, P.P. Shi, M.M. Zhao, et al., Chem. Mater. 33 (2021) 799–805.